2

CONF-8810201--2 Rev.

UCRL- 99716 Rev. 1
PREPRINT

DEC 7 1988

Reactive-element effect Studied Using Ion Implantation*

Wayne E. King and K. S. Grabowski**
Chemistry and Materials Science Department
Lawrence Livermore National Laboratory, Livermore, CA 94550
**Naval Research Laboratory
Washington, DC 20375

Invited paper submitted to the proceedings of the session on ENVIRONMENTAL DEGRADATION OF ION AND LASER BEAM TREATED SURFACES III: High Temperature Oxidation and Hot Corrosion at the 1988 TMS Fall Meeting, Chicago, IL, G. S. Was and K. S. Grabowski eds.

REVISED NOVEMBER 1988

REACTIVE-ELEMENT EFFECT STUDIED USING ION IMPLANTATION*

Wayne E. King

Chemistry and Materials Science Department
Lawrence Livermore National Laboratory, Livermore, CA 94550

K. S. Grabowski

Naval Research Laboratory
Washington, DC 20375

UCRL--99716-Rev.1

DE89 004774

Abstract

Implantation of reactive elements into metals that form chromia layers upon exposure to high temperature oxidizing environments has a very large effect on the growth rate of the oxide and adhesion of the oxide to the base alloy. We have investigated the effect of Y ion implantation on the high temperature oxidation of Fe-24Cr using Rutherford backscattering spectroscopy, secondary ion mass spectroscopy, and electron microscopy. Analytical tools have been applied to determine the spatial distribution of Y, the microstructure of the oxide, and contribution of oxygen transport to the oxidation process. Results are compared with similar experiments in Fe-Cr alloys with Y additions and with results of cation and anion tracer diffusion experiments.

*Work performed under the auspices of the US Department of Energy by the Lawrence Livermore National Laboratory under contract number W-7405-Eng-48 and by the U. S. Office of Naval Research.

Introduction

In this paper, we discuss the effect of reactive-element ion implantation on high temperature oxidation of high purity metal alloys that form Cr_2O_3 layers. The literature has reported that reactive-element implantation gives rise to the three beneficial effects often associated with the presence of reactive elements: stimulation of the early formation of a continuous single-phase protective oxide layer, reduction in growth rate of chromia, and enhanced oxide adhesion compared to addition-free materials. Ion implantation is a particularly important technique for treatment of metal surfaces that are subjected to high temperature oxidizing environments because (1) implantation of reactive elements can give rise to a larger reduction in oxide growth rate than observed in materials alloyed with reactive elements and (2) implantation provides an ideal technique to investigate the mechanisms that give rise to the reactive-element effect.

Because of our desire to concentrate in this paper on the impact of the ion implantation technique on elucidation of the mechanisms of the reactive-element effect, we will not discuss all of the important work that has been carried out in the past on the effect of ion implantation on oxidation resistance of metals. Instead, we refer the reader to other review articles on the subject (1-5). In addition, we refer specifically to the extensive work of Bennett and coworkers in Nb stabilized stainless steels which provides valuable information on the influence of reactive element implantation on the formation of multiphase oxide layers(6-11). We also cite, for the readers reference, work that has been carried out on complicated, commercial purity alloys(12, 13).

Previous workers have also investigated the effect of radiation damage that results from ion implantation on high temperature oxidation (eg see (3, 14)). These authors demonstrate that the presence of radiation induced defects in the near surface region can have a marked effect on the oxidation behavior of the base metals. However, the "chemical effects" of the reactive-element implantation were observed to be more important than the physical effects of the radiation damage. Therefore, we refer the reader to previous work on radiation effects and concentrate here on the chemical effects of the reactive element implant.

We have applied Rutherford backscattering spectroscopy, electron microscopy, and secondary ion mass spectroscopy to investigate the oxidation kinetics and elemental distributions that evolve during the oxidation of Fe-24Cr implanted with 1×10^{16}, 3×10^{16}, 1×10^{17} Y cm^{-2}. In this paper we discuss microstructural and microchemical evidence of the location and chemical state of the reactive element both in the oxide and in the metal. We compare and contrast the effects of ion implantation of reactive elements with the effects of alloying with reactive elements and discuss the impact of ion implantation on the elucidation of the mechanisms of the reactive-element effect.

Experimental

An alloy of Fe (Johnson-Matthey Chemicals Limited, Puratronic) 24 weight percent Cr (MRC Marz grade) was prepared by arc melting in an Ar atmosphere. Solidified buttons were cold rolled to 2mm thickness, wrapped in Ta, heat treated for one hour at 850°C, and finally cold rolled to 1 mm thickness. Samples were annealed at 1000°C. Surfaces of the annealed sample were final polished using 0.05μm Al_2O_3. The sample was given a short electropolish (5% Perchloric acid in Glacial acetic acid, 15-20°C, total of 2 min at 0.5-0.6 A-cm^{-2}). Analysis of the sample material revealed <400ppm total impurities. A typical analysis is shown in Table I.

Table I. Typical mass spectrographic analysis of impurity levels of samples used in this experiment in atomic parts per million.

Ag	ND(0.4)	N_2	180.
Al	Int.	Na	0.04
As	0.05	Ni	5.
Au	0.6	O_2	80.
C	24.	P	0.2
Ca	2.	Pb	0.1
Cd	ND(0.3)	Pd	Int.
Cl	0.2	Pt	0.05
Co	2.	S	3.
Cr	Major	Sb	0.2
Cu	2.	Sc	ND(0.02)
F	Int.	Si	8.
Fe	Major	Sn	3.
Ga	0.09	Ta	M(1.)
H_2	X	Ti	0.2
In	50.	V	0.06
K	0.07	W	0.2
Mg	ND(0.2)	Zn	ND(0.7)
Mn	0.5	Zr	0.5
Mo	0.4		

ND( ) - Not detected and less than amount in brackets.
Int. - Interference
X - Not looked for.
M - Contamination from instrument.

The sample, of dimension ~5 x 15 mm^2, was implanted with 150 keV Y ions at the Naval Research Laboratory. During implantation, the vacuum in the implantation chamber was ~1 x 10^{-6} torr and the sample was cooled to -25°C. Three regions of the sample were implanted each with a different ion dose: 1 x 10^{16}, 3 x 10^{16}, and 1 x 10^{17} cm^{-2}. We refer to these as the low, medium, and high doses respectively. Rutherford backscattering experiments were carried out before any oxidation and after incremental oxidation times of 5, 10, and 45 min at 1000°C in flowing oxygen. The sample was later oxidized at 900°C in ~10^{-1} torr $^{18}O_2$ after which secondary ion mass spectroscopy depth profiling was carried out to investigate the ^{18}O and Y depth distributions. Rutherford backscattering spectroscopy was carried out at the tandem accelerator facility in the Materials Science Division of Argonne National Laboratory using 1.770 MeV singly charged ^4He ions. The ion beam diameter at the specimen was ~1mm. There were ~5 x 10^7 oxide grains and ~1 metal grain in the analyzed area. Details of the analysis of the Rutherford backscattering data is given elsewhere(15).

Results and Discussion

Location of the implanted atomsin the as-implanted sample

The as-implanted Y depth distributions deduced from the RBS spectra are shown in Fig. 1. The magnitude of the peak in the Y depth distribution increases with implantation dose and moves toward the surface of the sample. This latter behavior is a consequence of the competition between implantation of Y into the sample and sputtering of Fe, Cr, and Y by the Y ions. As a result, not all of the implanted atoms are retained in the sample as shown in Fig. 2

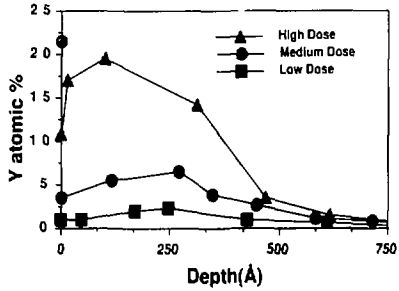

Figure 1. Y depth distributions for implantation doses of 1×10^{17}, 3×10^{16}, and 1×10^{16} cm^{-2} determined from RBS.

where we plot the retained Y dose as a function of the implanted Y dose. The straight line represents the case if no sputtering would occur. For the low, medium, and high dose implants, the surface composition is 2, 3, and 11 atomic percent Y respectively. The Y-Fe phase diagram is known to have limited solid solubility of Y in Fe and a stable phase Y_2Fe_{17} (16, 17). It is expected that during heating of the implanted samples to the oxidation temperature, formation of Y_2Fe_{17} is possible.

A number of previous experiments have been carried out to determine the lattice location and chemical state of rare-earth ions implanted in elements like Fe using ion channeling and angular—resolved perturbed angular correlation (18-21). Although the results of these studies are difficult to interpret, it appears that a strong interaction

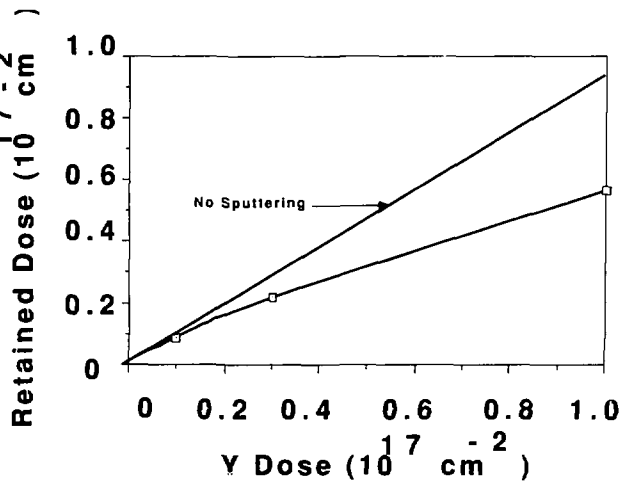

Figure 2. Retained Y dose as a function of implanted dose.

between reactive elements and oxygen occurs when O is present in the implanted region. When the reactive element is located near the sample surface, as in the case of low energy or high dose implantation, a strong interaction was also observed. This is most likely due to enhanced oxygen mobility in the highly defected implant region. We therefore expect rapid oxidation of the implanted atoms upon exposure of the sample to high temperature.

Oxidation kinetics

Figure 3 shows the Rutherford backscattering spectra and fits to the data after the three oxidation times for the 1 x 10^{16} cm $^{-2}$ implantation region. The effect on the spectra due to the increase of the oxide thickness with oxidation time can easily be seen. Figures 3 also shows marked roughening of the oxide/metal interface with oxidation time (see Ref. (15)). A similar effect was reported by Dearnaley(21). Therefore we describe the oxide as a pure oxide region and an interface region that is a mix of oxide and metal. Discussion of the interpretation of RBS spectra from oxidized samples can be found elsewhere(15). In Fig. 4 we show the oxide region thickness and interface region thickness obtained from fitting spectra for the three doses plotted as a function of time. Note that the interface region thickness is in some cases about the same as the oxide thickness. We therefore define the oxide thickness as the thickness of the pure oxide region plus one half of the thickness of the interface region. In Fig. 5 we plot the total oxide thickness as a function of time. An attempt was made to fit this data to parabolic diffusion controlled growth kinetics. Acceptable fits to parabolic growth could only be obtained if a very rapid formation of the initial oxide layer was assumed ie

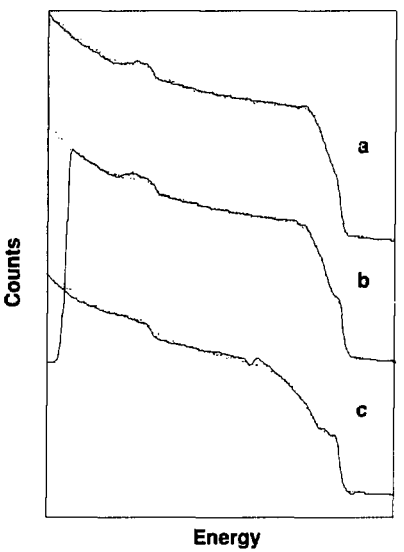

Figure 3. Rutherford backscattering spectra from 1 x 10^{16} cm $^{-2}$ samples oxidized for (a) 5 min., energy range 374 to 1539 keV (b) 15 min., energy range 388 to 1540 keV, and (c) 1 hour, energy range 385 to 1538 keV. Data are shown as points, fit to data is shown as solid line.

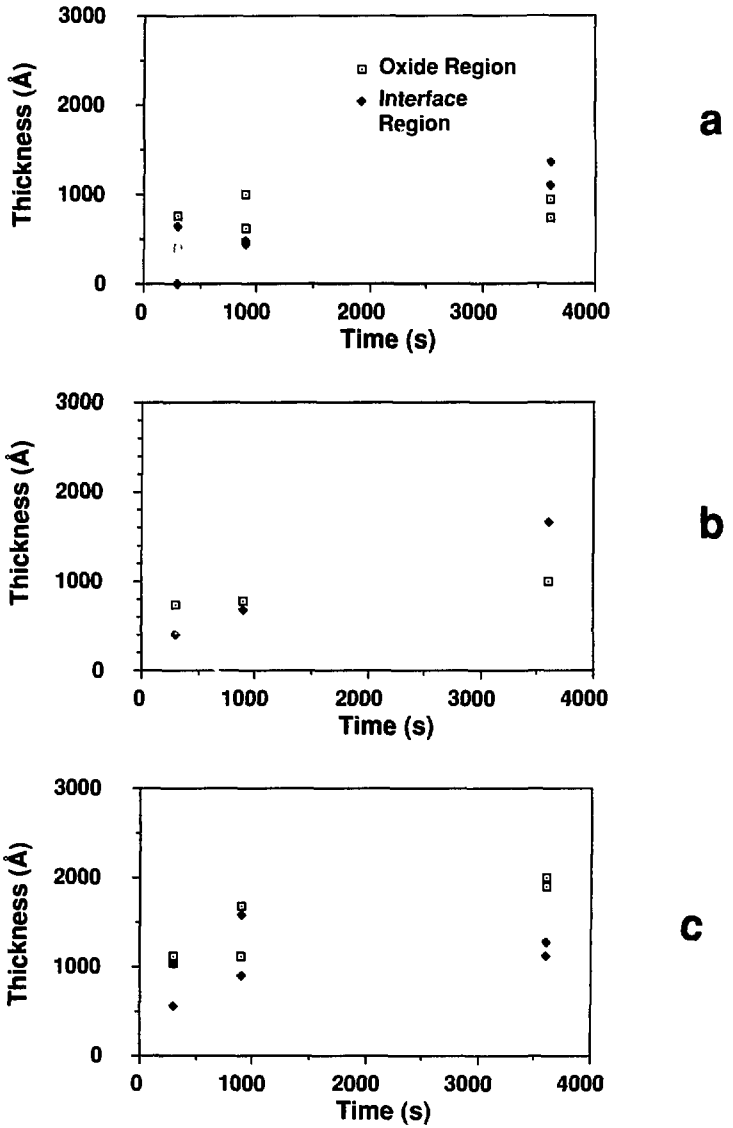

Figure 4. Oxide region thickness and interface region thickness as a function of time deduced from Rutherford backscattering data of (a) 1 x 10^{16} cm $^{-2}$, (b) 3 x 10^{16} cm $^{-2}$, and (c) 1 x 10^{17} cm $^{-2}$.

$$x^2 = k_p t + x_0^2, \quad (1)$$

where x is the oxide thickness, x_0 is the initial rapidly formed oxide thickness, k_p is the parabolic rate constant, and t is time. Acceptable fits were obtained for the low and medium dose cases and are shown in Table II and Fig. 5. The high dose case could not be fit with such a simple model. Note that these values of x_0 correspond to complete consumption of Cr atoms from about the first 1300Å of the base alloy. This depth exceeds the Y implantation depth. We do not imply that the simple function of Eq. 1 describes the operative mechanism in the oxidation process. The actual mechanism is believed to be the sum of three terms: a parabolic term for oxidation of the implanted atoms (ie internal oxidation), a parabolic term for oxidation of the base metal, and a term that accounts for consumption of the limited quantity of implanted atoms. This model neglects the effect of interface roughening. Because we have data at only three oxidation times, it is not possible to fit such a complex model. Roughening of the interface further complicates analysis of the experimental data. As a result, the k_p values that are shown in Table II are intended only to indicate that the steady-state oxide growth is very slow compared with both addition-free alloys and alloys with Y additions.

Table II. Values for k_p and x_0 deduced from fits to the low and medium dose data for oxidation at 1000°C in flowing oxygen.

Dose (cm^{-2})	k_p (cm^2s^{-1})	std. error (cm^2s^{-1})	x_0 (cm)	std. error (cm)
1×10^{17}	5.36×10^{-14}	7.49×10^{-15}	5.69×10^{-6}	2.56×10^{-6}
3×10^{16}	7.41×10^{-14}	2.61×10^{-15}	7.97×10^{-6}	1.32×10^{-6}

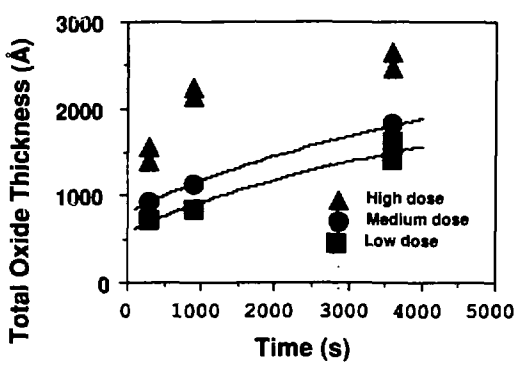

Figure 5. Total oxide thickness as a function of time deduced from Fig. 4 for doses of 1×10^{17}, 3×10^{16}, and 1×10^{16} cm^{-2}. Fits to the data are plotted as solid lines.

Location of the implanted atoms in the oxidized sample

Various techniques have been applied in the past to investigate the distribution of the reactive-element implant in the oxide layer and in the base metal. Two observations are generally reported: for sufficiently high implantation doses, the implanted atoms are primarily found near the oxide/gas interface and for lower doses, the implanted atoms are primarily found near the oxide/metal interface(6, 14, 15, 21-27). Similar observations have in the past generally been attributed to a change in the oxidation mechanism from predominantly cation diffusion at low doses to predominantly anion diffusion at high doses. However, we feel strongly that conclusions from inert marker experiments and inferences based on the location of the reactive element in the oxides are subject to errors, as clearly demonstrated by Young and deWit(28, 29). Resolution of this problem awaits $^{16}O/^{18}O$ SIMS or nuclear reaction analysis experiments on fully-dense oxide layers.

Figure 6 shows the Y depth distribution for the three oxidation times for the three doses 1×10^{16}, 3×10^{16}, and 1×10^{17} cm^{-2}. The horizontal bars define the thickness of the interface region. All plots show a slight enhancement in Y concentration at the surface of the oxide. Below the surface of the oxide, the Y concentration drops to nearly zero before rising to a peak. For the highest dose implantation case, results indicate that additional Y was concentrated about 2000Å below the oxide surface after 5 min and 15 min oxidations. However, this high dose result is suspect. The Y backscattering signal at this greater depth is buried under Fe and Cr signals which vary unevenly with energy, adding uncertainty to the fitting results. These difficulties do not apply to the Y distribution for depths up to about 1000Å of oxide, since the Y signal is free of Fe and Cr background signals up to that depth.

The peak in the Y distribution for the low and medium dose samples is located near the oxide/metal interface for all oxidation times. The first peak in the Y distribution in the high-dose case was always located within the oxide, ~800Å below the oxide surface which was well removed from the oxide/metal interface for the longer oxidation times. These points are illustrated in Fig. 7 where we plot the Y peak position relative to the oxide surface as a function of oxide thickness. It is clear from this figure that after the initial rapid oxidation, the oxide thickens toward the surface side of the peak in the Y distribution for the low and medium dose cases because the Y peak position relative to the oxide surface increases as a function of oxide thickness. In the high dose case, the oxide thickens below the peak in the Y distribution as evidenced by the invariance of the peak position with oxide thickness.

After oxidation most of the Y was found in the oxide and the interface region. Upon integration of the Y depth distributions from the oxide/gas interface to the interface between the oxide and the interface region and through the interface region, we found that the amount of Y in all the oxides increased linearly with retained dose. A point that is less clear is how much Y was left in the metal. Collins et al.(14, 30) found in oxidation of Y implanted Cr that after oxidation, and removal of the oxide by polishing, the sample still persisted to exhibit reduced oxide growth rate possibly implying that some reactive element was left in the metal after polishing. Although we cannot say with complete generality, we know that in some cases (particularly in the short oxidation times) Y was still present in the metal after oxidation.

Hondros has shown that for a variety of segregants in a variety of matrices, the variation in concentration of solute with distance from a grain boundary is nearly independent of solute or matrix as shown in Fig. 8(31). One of the segregation curves in Fig. 8 is for Y segregation to grain boundaries in Al_2O_3(32). Yttrium segregation to grain

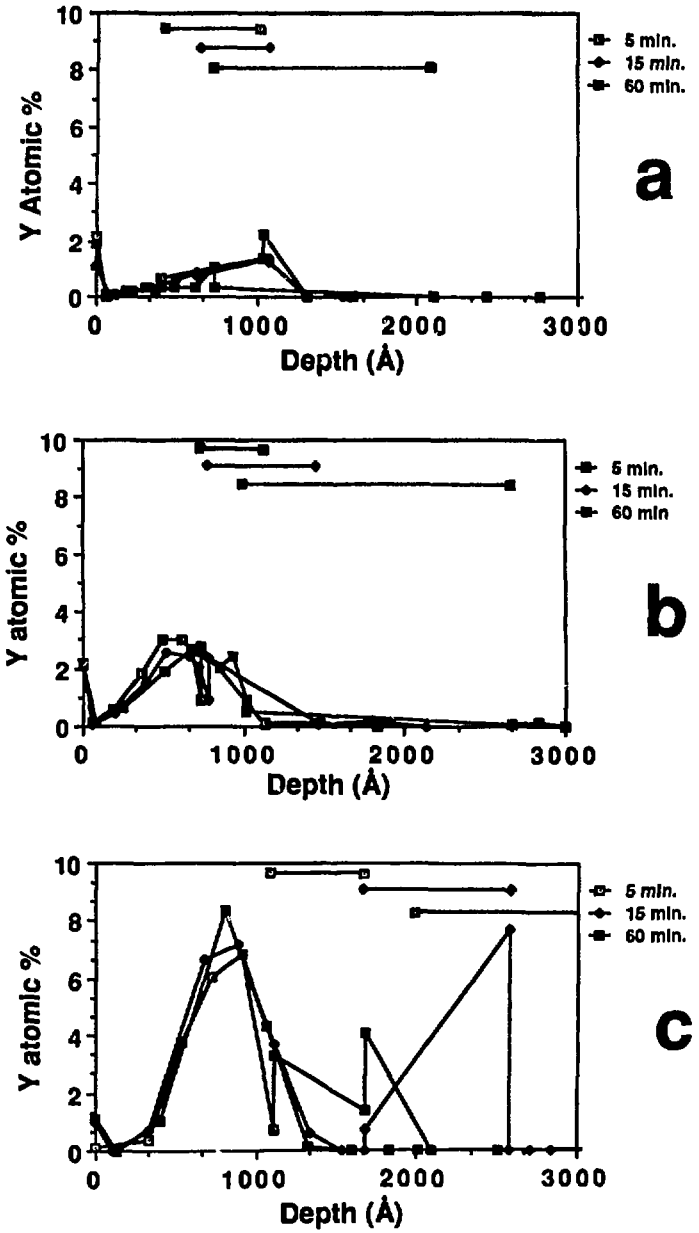

Figure 6. Y depth distribution for the three oxidation times for the three doses (a) 1 x 10^{16}, (b) 3 x 10^{16}, and (c) 1 x 10^{17} cm^{-2}. Horizontal bars define the interface region.

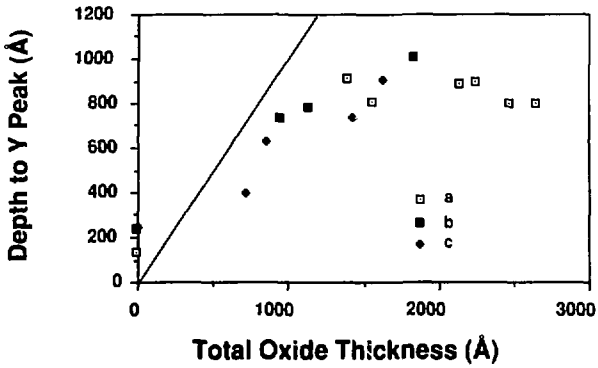

Figure 7. Depth within oxide of peak in Y distribution relative to the oxide surface as a function of oxide thickness

boundaries in Cr_2O_3-0.09 weight percent Y_2O_3 has been observed on fracture surfaces of polycrystalline samples fractured intergranularly at 1200°C in compression(33). Based on this evidence, we expect that in the oxide layers, the implanted atoms are segregated to the oxide grain boundaries.

Pryzbylski et al. have applied high spatial resolution x-ray energy dispersive spectroscopy to determine the location of implanted Y (70 keV, 2 x 10^{16} cm $^{-2}$) in the oxide layer formed on Co-45 weight percent Cr(23, 34-36). By using a very small electron probe on thin plan sections of the oxide layer, Pryzbylski et al. have been able to identify that Y is segregated at monolayer concentrations to the grain boundaries in the growing Cr_2O_3 layer. The measurement of detectable amounts of Y at oxide grain boundaries is in contrast to observations in oxides grown on alloys where the reactive element has proved to be rather difficult to detect(37).

Pryzbylski et al. have also reported that perovskite $YCrO_3$ precipitates form in the growing oxide layer(38). These precipitates were identified using convergent beam electron diffraction. While the present authors have been unable to confirm the indexing scheme reported by Pryzbylski et al., we agree that it is possible to index the patterns as $YCrO_3$. This conclusion is in agreement with what would be expected from the equilibrium phase diagram for the Cr_2O_3-Y_2O_3 system. However, the existence of the perovskite particles is an interesting observation in light of the rather high probability that the implanted atoms internally oxidize to Y_2O_3 before incorporation in to the growing oxide layer where it would then have to undergo a solid state phase transformation to $YCrO_3$ at a rather low temperature.

The above information leads us to hypothesize that reactive element ion implantation impacts oxidation behavior in two distinct ways: (1) when the near-surface concentration of implanted reactive element in the alloy is below a critical level, the majority of the implanted element will be found near the oxide/metal interface following oxidation and (2) above this critical level, the majority of the implanted element will be found near the oxide/gas interface. The critical concentration is probably related to the formation of a second phase in the scale, which may be related to the formation of a second phase in the alloy, either during implantation or upon heating the sample for oxidation. This is reasonable since only 10.53 at. % Y is necessary to completely form Y_2M_{17} where M can be Fe, Ni, or Co, and the solubility limit of Y is expected to be less than 1 at. % for chromia- scale forming alloys(17, 39).

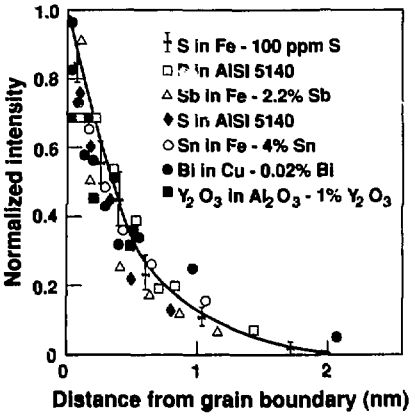

Figure 8. Grain boundary segregation measured in a number of systems (31).

The near-surface concentration of implanted atoms is a function of both ion dose and ion energy. By reviewing the literature(14, 15, 21-27), we have established the ion dose required to produce the critical level of reactive element for a number of ion implantation energies. This relation is plotted in Fig. 9. Evaluation of Y composition profiles calculated for each of the experimental cases indicates that the critical concentration could be an Y concentration at the surface of about 1 at. %, or a peak Y concentration of about 6 at. %. Curves for both of these criteria calculated for Y implantation of Fe-24Cr are shown in Fig. 9. Beyond these concentrations it is likely that either precipitation at the surface could begin, or nearly 50 vol. % of the intermetallic ytride could form beneath the surface. It would not be surprising for such effects to influence secondary phase formation in the scale. Formation of these precipitates in the alloy of course depends on the thermal history of the implanted samples and the opportunity for internal oxidation of the Y. Some deviations from the guidelines in Fig. 9 should be expected. We propose that for doses above the critical dose, the effect that is observed is not the reactive-element effect by its most strict definition. At these high doses, we believe that second phase formation in the oxide is likely, an occurance that is not always observed in alloy systems (40) (except perhaps in the oxide located immediately over rare-earth yttride precipitates in the metal) and which is not required for the reactive-element effect to be operative.

Composition of the oxide layer in implanted samples

Analyses of the RBS spectra show that all of the oxide layers are composed of a thin (447± 138Å) outer layer of Cr_2O_3 containing 7.0 ± 3.5 atomic percent Fe near the surface. This is illustrated in Fig. 10 where we plot the Fe and Cr depth distribution corresponding to the high dose implant after 1 hour of oxidation. The presence of Fe in the oxide is expected in alloys oxidized in oxygen partial pressures that are high enough to oxidize Fe. In separate experiments, oxide compositions of Fe-13Cr oxidized in Ar-7%O_2 and in H_2–H_2O at 700°C have been studied by RBS. Iron-containing oxides were observed for the oxidation in Ar–7%O_2 as shown in Fig. 11a. However, in the H_2–H_2O case (very low oxygen partial pressure) almost no Fe was observed in the oxide (Fig. 11b).

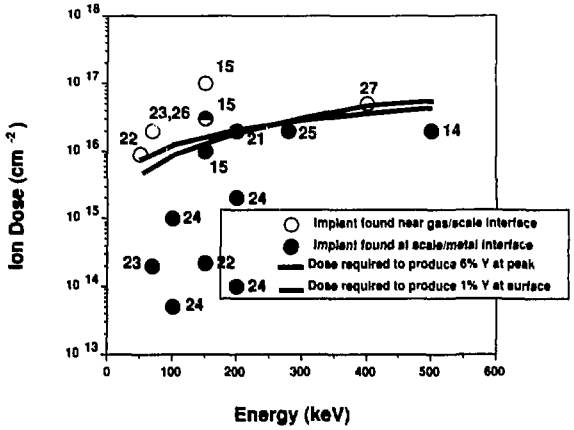

Figure 9. Y and Ce ion dose as a function of energy, solid points indicate that the implant was found at the scale/metal interface, open points indicate that the implant was found near the scale/gas interface.

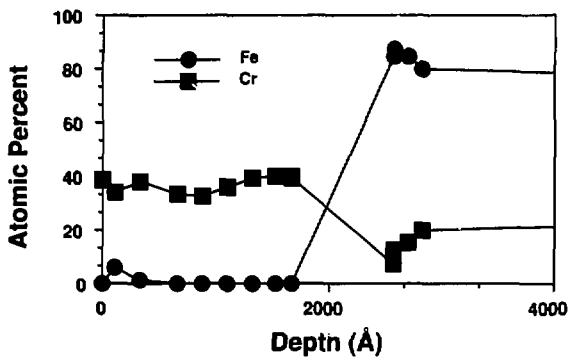

Figure 10. Fe and Cr depth distribution as deduced from the high dose implant after 1 hour of oxidation.

Composition of the oxide layer in alloyed samples

We have used RBS and SIMS to investigate the composition of oxide layers formed on alloys of Fe-13Cr, Fe-24Cr, Fe-13Cr-0.3Y, and Fe-24Cr-0.3Y that were oxidized in Ar-7%O_2 and in H_2-H_2O at 700°C. Figure 12 shows an ion-induced secondary-electron image of the surface of Fe-13Cr-0.3Y oxidized in Ar-7%O_2 acquired using a 30 keV Ga^+ ion gun on a Vacuum Generators high spatial resolution analytical ion microscope. The surface contains a smooth surface oxide and nodules protruding from the surface. SIMS confirmed that the smooth oxide was Cr_2O_3. Figure 13

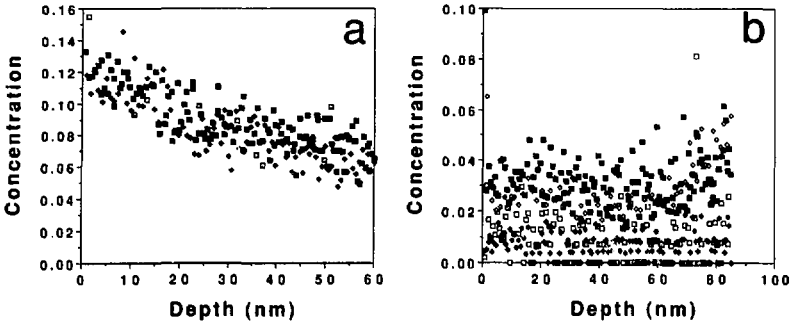

Figure 11. (a) SIMS Fe depth profile through oxide layer on Fe-13Cr alloy oxidized in Ar-7%O_2 at 700°C. (b) SIMS Fe depth profile through oxide layer on same alloy oxidized in H_2-H_2O at 700°C. Each symbol represents a different depth profile.

shows a depth profile through one of the nodules in Fig. 12. These oxide nodules are high in Fe compared with the smooth oxide. Further, each nodule has Y at its center as can be seen in Fig. 13. We believe that these nodules lie on top of $Y_2(Fe,Cr)_{17}$ precipitates in the base metal. During oxidation, these yttrides in this relatively low-Cr alloy apparently oxidize very rapidly compared to the surrounding alloy thus forming Y-rich nodules. We believe that this behavior is similar to the transient oxidation behavior observed in the high dose implantation where the Y concentration at the sample surface is comparable to that of $Y_2(Fe,Cr)_{17}$.

Nodule formation is not observed in Fe-24Cr-0.3Y alloys as shown in Fig. 14a, the ion-induced secondary-electron image from the surface of an oxidized Fe-24Cr-0.3Y alloy. This image exhibits small areas of light contrast. In parallel with the acquisition of this secondary-electron image, a Y secondary-ion image was also acquired. Figure 14b shows a representation of the Y distribution overlayed on the secondary-electron image of Fig. 14a. Image points where Y was detected are colored black. Note that the Y-rich regions correspond to the areas of light contrast in Fig. 14a. Images were acquired as a function of depth during sputtering with the 30 keV Ga^+ ion source. Continuous Y rich regions of oxide were observed throughout the scale thickness indicating that Y is present in the scale in columns located atop the yttrides in the base metal. If Y was present in other parts of the oxide film, it was at substantially lower concentrations than over the yttrides. This heterogeneous distribution is in sharp contrast to that produced in ion implantation, at least for doses below the critical level as shown in Fig. 9. It should be pointed out that the oxide thickness in the Y-rich regions appeared to be the same as in the other regions of the scale.

Oxygen transport in the oxide.

SIMS depth profiling was carried out at NRC Canada after 1 hour further oxidation at 900°C in ^{18}O. One of these data sets is shown in Fig. 15 where we plot the concentration of mass 71 relative to mass 69+71 as a function of sputtering time. The sputtering beam current was one half as large for the high dose sample as for the other two samples. A peak of the $Y^{18}O$ signal occurred after about 20 to 25 minutes of sputtering for the low and medium dose cases and after about 45 minutes for the high dose case, indicating the position of the peak in the Y distribution. These profiles

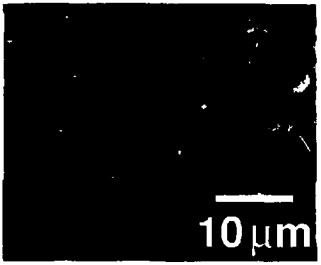

Figure 12. Ion-induced secondary electron image of surface of Fe-13Cr-0.3Y alloy oxidized in Ar-7%O_2 at 700°C.

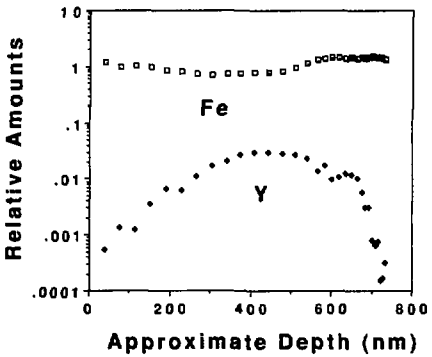

Figure 13. SIMS depth profile through a single nodule in Fig. 12.

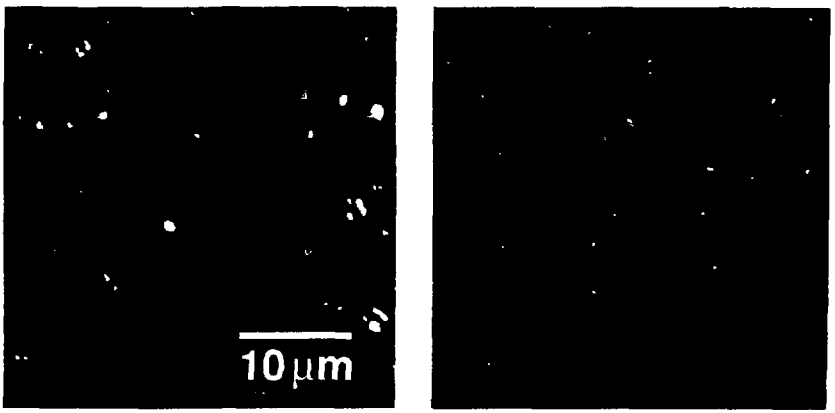

Figure 14. (a) Ion induced secondary electron image of surface of Fe-24Cr-0.3Y oxidized in Ar-7%O_2 at 700°C. (b) Same as (a) with Y secondary ion image in black.

indicate that the highest ^{18}O concentration occurred at the surface, and was quite low in the bulk of the oxide. As the Y implantation dose increased, the ^{18}O content in the oxide decreased. At the highest Y dose, a buildup of ^{18}O was observed to coincide with the peak in the Y distribution. This data suggests that Y reduces the inward transport of oxygen through a chromia scale, and at high enough concentrations can trap a significant portion of the inwardly migrating O. Without further experimentation, it is impossible to establish the growth mechanism of the oxide layers.

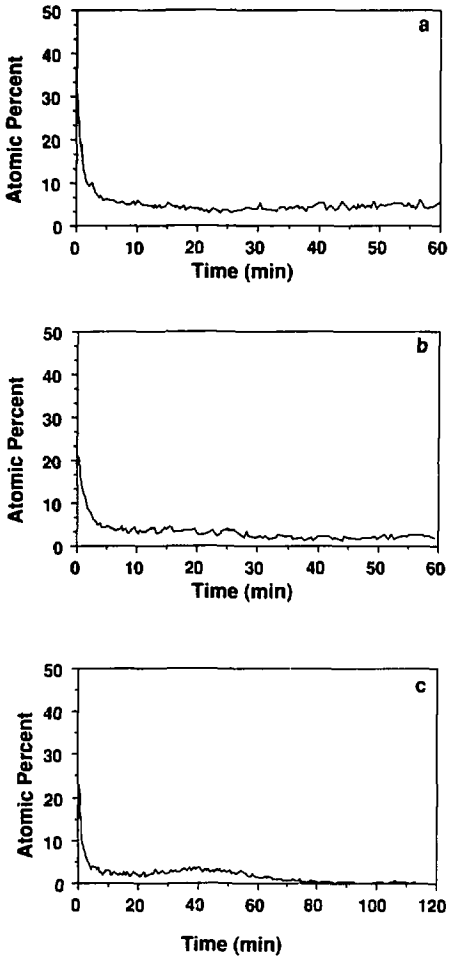

Figure 15. SIMS depth profiles for mass 71 ($Cr^{18}O$) for the (a)1 x 10^{16}, (b)3 x 10^{16}, and (c) 1 x 10^{17} cm^{-2}. The sum of $Cr^{16}O$ and $Cr^{18}O$ signals is 100%.

Relation of the present results to transport in the oxide.

If oxidation proceeds by diffusion along short circuit paths like grain boundaries in the oxide layer, the equation that describes the usual diffusion controlled oxidation kinetics,

$$x^2 = k_p t \qquad (2)$$

where x is oxide thickness, t is time, and k_p is the so-called parabolic rate constant, still holds, but the expression for k_p must be modified to reflect the fact that grain-boundary diffusion is the dominant mechanism of mass transport in the oxide(41):

$$k_p \approx (\text{const}) D'\delta/g. \qquad (3)$$

, D' is the grain boundary diffusion coefficient, δ is the effective grain boundary width, and g is the average grain diameter. If cation diffusion is the rate controlling mechanism, the constant in Eq. 3 is of the order 50, the exact value depends on the oxygen partial pressure dependence of D'δ. The parabolic rate constant is a function of both grain-boundary diffusivity and oxide grain size.

To compare the present results from Table II and literature data(22, 37, 42-45) on growth of Cr_2O_3 (22, 37, 42, 43) with cation and anion diffusion measurements (44, 45), we convert the experimental values of k_p to values of D'δ using the procedure described by Park et al.(45) In that work, the assumption was made that the contribution of anion diffusion to the growth of Cr_2O_3 films was negligible. In a recent study by King and Park,(44) anion diffusivities in the lattice and along grain boundaries were measured on sintered polycrystals of Cr_2O_3 and Cr_2O_3–0.09 weight percent Y_2O_3 at 1100°C and at the oxygen partial pressure corresponding to that of the Cr/Cr_2O_3 equilibrium at that temperature. Results demonstrated that under the same conditions, anion diffusion is significantly faster than cation diffusion. However, because the oxygen partial pressure dependence of anion diffusion in Cr_2O_3 is unknown, it is not possible to convert values of k_p to D'δ based on this new information. Therefore we calculate values of D'δ assuming that cation diffusion is the operative mechanism and compare the results with values of D'δ measured from cation and anion diffusion experiments. The results of these calculations are given in Table III.

Figure 15 shows a plot of D'δ versus inverse temperature for the available literature data. Also included in Fig. 16 are the D'δ values from cation(45) and anion(44) tracer diffusion studies. It is important to note that the values for D'δ deduced from k_p measurements are spread over 2 orders of magnitude. Also, all values for D'δ, except those deduced from the current implantation experiment and the experiments of Pivin et al.(22), are higher than the values measured for cation grain boundary transport in Cr_2O_3 and Cr_2O_3 doped with Y_2O_3 at 1100°C. This indicates that cation grain boundary diffusion is far too slow to explain the observed oxide growth rates in unimplanted samples. However, these data are consistent with the anion grain boundary diffusion data of King and Park(44). The oxidation rates of the implanted samples in this study and in that of Pivin et al.(22) are consistent with rate control by cation grain boundary diffusion.

In the past, we have analyzed the results of oxidation experiments by Caplan and Sproule(46) in terms of cation grain boundary diffusion(15, 44, 45, 47). Because Caplan and Sproule measured the growth rate of the slowest growing oxide grains on their samples, they speculated that growth of these grains was controlled by bulk diffusion. In light of the results of King and Park(44), we have reanalyzed the Caplan and Sproule data assuming that growth of these grains

Table III. Values for D'δ Determined from literature data.

T (°K)	$p_{O_2}(i)$ (Pa)	$p_{O_2}(o)$ (Pa)	k_p (cm^2s^{-1})	g (μm)	D'δ (cm^3s^{-1})	Ref.
1173	1.92×10^{18}	1.00×10^{5}	1.03×10^{13}	1.0	4.92×10^{19}	21
1173	1.92×10^{18}	1.00×10^{5}	1.03×10^{13}	5.0	2.46×10^{18}	21
1173	1.92×10^{18}	1.00×10^{5}	2.21×10^{14}	0.1	1.05×10^{20}	21§
1173	1.92×10^{18}	1.00×10^{5}	2.21×10^{14}	0.3	3.61×10^{20}	21§
1173	1.92×10^{18}	1.00×10^{5}	7.37×10^{15}	0.1	3.52×10^{21}	21§
1173	1.92×10^{18}	1.00×10^{5}	7.37×10^{15}	0.3	1.06×10^{20}	21§
1173	1.92×10^{20}	1.00×10^{5}	4.00×10^{12}	0.1	5.48×10^{17}	37
1173	1.92×10^{20}	1.00×10^{5}	2.50×10^{12}	0.1	1.19×10^{18}	37'
1273	8.23×10^{18}	1.00×10^{5}	5.36×10^{14}	0.11	1.88×10^{20}	§§
1273	8.23×10^{18}	1.00×10^{-1}	7.33×10^{13}	0.5	2.23×10^{18}	42
1273	8.23×10^{18}	1.00×10^{5}	7.41×10^{14}	0.14	3.30×10^{20}	§§
1273	8.23×10^{18}	1.00×10^{-9}	7.33×10^{13}	0.5	2.36×10^{18}	42
1298	3.24×10^{17}	5.00×10^{5}	1.00×10^{-10}	0.15	1.91×10^{19}	37
1298	3.24×10^{17}	5.00×10^{5}	1.80×10^{11}	0.15	9.37×10^{18}	37'
1348	4.30×10^{16}	1.00×10^{5}	2.90×10^{10}	1.5	8.99×10^{16}	43
1373	-	-	-	-	2.10×10^{17}	44'
1373	-	-	-	-	2.25×10^{19}	45'''
1373	-	-	-	-	7.20×10^{18}	44''
1373	-	-	-	-	8.61×10^{20}	45''
1473	1.28×10^{13}	7.00×10^{-2}	6.50×10^{11}	3.0	8.68×10^{16}	43

' Cr-Y alloys
'' ^{51}Cr diffusion in Cr_2O_3
''' ^{51}Cr diffusion in Cr_2O_3-Y_2O_3
' ^{18}O diffusion in Cr_2O_3-Y_2O_3
'' ^{18}O diffusion in Cr_2O_3
§ Y ion implanted
§§ This Work

is controlled by bulk diffusion of anions. This result along with other measured anion bulk diffusivities are plotted in Fig. 17(44, 48, 49). Note the result of Caplan and Sproule at 1100°C is within the error bar of the anion tracer diffusion in pure Cr_2O_3 result of King and Park. This analysis assumes that anion diffusion has the same oxygen partial pressure depencence as cation diffusion. The cation diffusion results of Park et al.(45) and Atkinson and Taylor(50) are also shown in Fig. 17. These results show that cations in chromia diffuse orders of magnitude slower than anions in the bulk.

Conclusions

Ion implantation of reactive elements into metals that form chromia upon high temperature oxidation gives rise to a reduction of oxide growth rate, enhanced oxide adhesion, and early formation of a continuous, single-phase chromia layer. A transient oxidation behavior is observed that appears to be associated with rapid oxidation through the implanted region. There appears to be a critical implantation dose above which a change in the oxidation behavior of the alloy is observed. Below the critical dose, the implanted atoms are located near to the oxide/metal interface. In this regime, the reactive-element effect due to implantation of energetic ions seems to be similar to the effects observed due to alloying with reactive elements except that in alloys the reactive element is not found in such high concentrations in the oxide layers (except over yttrides) as in implanted samples and implantation gives rise to a larger reduction in growth rate compared to alloying. Below the critical dose, ion implantation produces a laterally uniform distribution

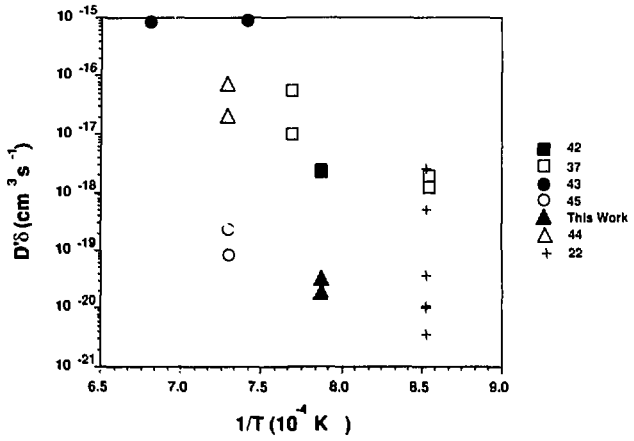

Figure 16. D'δ values deduced from previous experiments plotted as a function of inverse temperature.

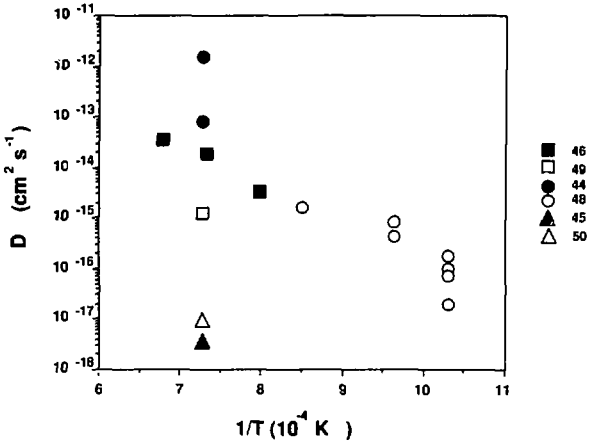

Figure 17. Anion bulk diffusion values deduced from previous experiments plotted as a function of inverse temperature.

of reactive element whereas alloying often results in second phase formation in the base metal. Above the critical dose, the implanted atoms are found near to the gas/oxide interface. Additionally, second phase formation in the scale probably occurs. This is most likely due to the very rapid oxidation of the high implant concentration region as observed in nodule formation in Fe-13Cr-0.3Y alloys. Chromia formed on unimplanted alloys grows at rates consistent with anion grain boundary diffusion. Whereas, chromia on implanted alloys grows at rates consistent with cation grain boundary diffusion. SIMS data suggest that Y reduces the inward transport of oxygen through a chromia scale, and at high enough concentrations can trap a significant portion of the inwardly migrating O.

Ion implantation is certain to continue to have a large impact in elucidation of the mechanisms of the reactive-element effect. This is primarily because implantation allows the reactive element to be injected in a measurable amount at a measurable location. The uniform implant distribution in the plane of the sample surface greatly simplifies the problem. However, we must keep in mind that in alloys the effect is present with very low concentrations of reactive element in the oxide layer. Many investigators suggest that implantation alters the oxidation mechanism between control by anion and cation transport. Implantation experiments will play a key role in determining the operative mechanisms.

Does ion implantation give rise to the reactive-element effect as defined by Whittle and Stringer(51)? The key to answering this may be in the rather large amount of reactive element that is observed in scales. If the large amount of reactive element in the scale gives rise to a secondary mechanism, then this is not the classical reactive-element effect. However in the dose ranges below the critical dose, the effects are too similar to that observed in alloys to conclude that this is not the reactive-element effect. But it could be that the mechanisms are not the exactly the same. If the mechanisms for the reactive-element effect in alloys is the same as in implanted metals, then we must find reactive element at grain boundaries in oxides scales grown on alloys with reactive element additions

We have investigated the effect of Y implantation on the high temperature oxidation of Fe-24Cr. In the case of the low and medium dose samples, Y was observed to be located near the metal/oxide interface even though the metal/oxide interface has passed through the original implanted depth. In the high dose case, an Y rich layer was observed within the oxide layer. A critical dose vs implantation energy relation was proposed to better define this change in behavior. All samples were observed to form a Cr_2O_3 layer very quickly, followed by very slow growth. Recent experiments motivate us to look to cation diffusion as the operative mechanism for growth of these oxide scales. The growth rate on the low and medium dose regions was nearly as slow as that predicted from recent cation grain boundary diffusion measurements on polycrystalline Cr_2O_3. However, the absolute value of the parabolic rate constant is uncertain due to operation of more than one mechanism and roughening of the metal oxide interface. However the growth rates were consistent with previous studies.

Acknowledgements

The authors gratefully acknowledge their collaboration with D. F. Mitchell, R. Hussey, P. Baldo, and J. Hamilton.

References

1. C. R. Clayton, "Chemical effects of ion implantation: Oxidation, Corrosion, Catalysis," Surface Alloying by Ion, Electron, and Laser Beams, ed. L. E. Rehn, S. T. Picraux and H. Wiedersich (Metals Park, OH: ASM, 1987), 325-355.

2. G. Dearnaley, "Alteration of oxidation and relate properties of metals by ion implantation," Nucl. Instrum. Methods, 182/183, (1981) 899-914.

3. G. Dearnaley, "Thermal Oxidation," Ion Implantation, 18, ed. J. K. Hirvonen (New York: Academic Press, Inc., 1980), 257-320.

4. K. S. Grabowski and L. E. Rehn, "Ion implantation Effects on the Thermal Oxidation of Metals," Corrosion of Metals Processed by Directed Energy Beams, ed. C. R. Clayton and C. M. Preece (New York: The Metallurgical Society of AIME, 1982), 23-52.

5. M. J. Bennett, "The role of ion implantation in high temperature oxidation studies," High Temperature Corrosion, NACE-6, ed. (Houston: National Association of Corrosion Engineers, 1983), 145-154.

6. J. E. Antill, M. J. Bennett, R. F. A. Carney, G. Dearnaley, F. H. Fern, P. D. Goode, B. L. Myatt, J. F. Turner and J. B. Warburton, "The effect of surface implantation of yttrium and cerium upon the oxidation behavior of stainless steel and aluminized coatings at high temperatures," Corros. Sci., 16, (1976) 729-745.

7. M. J. Bennett, M. R. Houlton and G. Dearnaley, "The influence of the surface ion implantation of aluminum and cerium upon the oxidation behavior of a Fe-15%Cr-4%Al Fecralloy stainless steel, in air, at 1100°C," Corros. Sci., 20, (1980) 69-72.

8. M. J. Bennett, G. Dearnaley, M. R. Houlton and R. W. M. Hawes, "The influence of cerium and yttrium implantation upon the oxidation behavior of a 20%Cr/25%Ni/Nb stabilised stainless steel, in carbon dioxide, at 825°C," Ion Implantation into Metals, ed. V. Ashworth, W. A. Grant and R. P. M. Procter (Elmsford, NY: Pergamon Press, 1982), 264-276.

9. M. J. Bennett, B. A. Bellamy, G. Dearnaley and M. R. Houlton, "The influence of europium, lanthanum, scandium, and ytterbium ion implantation upon the oxidation behavior of a 20%Cr/25%Ni/Nb stabilised stainless steel, in carbon dioxide, at 825°C," (Paper Presented at 9th International Congress on Metallic Corrosion, Ottawa, Ontario:NRCC, 1984), 416.

10. M. J. Bennett, B. A. Bellamy, C. F. Knights, N. Meadows and N. J. Eyre, "Improvement by cerium and yttrium ion implantation of the oxidation behavior of a 20Cr-25Ni Niobium-stabilized stainless steel in CO_2," Mater. Sci and Eng., 69, (1985) 359-373.

11. M. J. Bennett, J. A. Desport and P. A. Labun, "Yttrium location and chemical state in the scale formed on Y-implanted 20%Cr/25%Ni/Nb stabilized stainless steel in carbon dioxide at 825°C," (Paper Presented at 42rd Meeting of the Electron Microscopy Society of America, 1985), 270.

12. M. Slater, W. A. Grant and G. Carter, "Some effects of implantation into metals on oxidation processes Part I: The influence of Y^+ and Dy^+ implantation upon the oxidation behavior of an Incoloy Alloy MA956 and an austenitic steel," Radiat. Eff., 82, (1984) 239-248.

13. M. Slater, "Some effects of implantation into metals on oxidation processes Part II: the influence of Dy^+ implantation on the oxidation behavior of Ni and stainless steel at 500°C," Radiat. Eff., 82, (1984) 249-261.

14. R. A. Collins, S. Muhl and G. Dearnaley, "The effects of rare earth impurities on the oxidation of chromium," J. Phys F:Metal Phys., 9, (1979) 1245-1259.

15. W. E. King and K. S. Grabowski, "Rutherford backscattering study of high temperature oxidation of Y implanted Fe-24Cr," submitted to Oxid. Met., (1988)

16. R. Ayer, J. C. Scanlon, T. A. Ramanarayanan, R. R. Mueller and R. Petkovic-Luton, "Crystal structure of intermetallic phase in Fe-20Cr-4Al-0.5Y alloy by convergent beam electron diffraction," J. Mater. Res., 2, (1987) 16-27.

17. W. G. Moffatt, The Handbook of Binary Phase Diagrams (Schenectady, NY: Genium Publishing Corporation, 1988).

18. L. Thomé, H. Bernas, J. Chaumont, F. Abel, M. Bruneaux and C. Cohen, "Search for internal oxidation in rare earth-implanted iron," Phys. Lett., 54A, (1975) 37-38.

19. L. Thomé, H. Bernas, F. Abel, M. Bruneaux, C. Cohen and J. Chaumont, "Study of the rare-earth-oxygen interaction in iron by lattice location and perturbed-angular-correlation experiments," Phys Rev. B, 14, (1976) 2787-2794.

20. L. Thomé, H. Bernas, J. Chaumont, F. Abel, M. Bruneaux and C. Cohen, "Search for the internal oxidation on rare earth implanted iron," Hyperfine Interactions, 2, (1976) 350.

21. G. Dearnaley, T. Laursen and J. L. Whitton, "A Rutherford Bascattering-channelling study of yttrium-implanted stainless steel before and after oxidation," Mater. Sci. and Eng., 90, (1987) 191-196.

22. J. C. Pivin, C. Roques-Carmes, J. Chaumont and H. Bernas, "The influence of yttrium implantation on the oxidation behavior of 67Ni-33Cr, Fe-43Ni-27Cr and Fe-41Ni-25Cr-10Al Refractory Alloys," Corros. Sci., 20, (1980) 947-962.

23. K. Przybylski, "The influence of yttrium on the growth mechanism of Cr_2O_3 scale formed on Cobalt-base alloys," (Paper Presented at 10th International Symposium on the Reactivity of Solids, Dijon (France), 1984), 241-246.

24. F. Cosandey, N. Patibandla and B. Wilkens, "A Rutherford backscattering study of oxide nucleation and growth kinetics of Ce implanted Ni-20Cr Alloys," Norman L. Peterson Memorial Symposium - Oxidation of Metals and Associated Mass Transport, ed. M. A. Dayananda, S. J. Rothman and W. E. King (Warrendale, PA: The Metallurgical Society, Inc., 1987), 227-248.

25. C. H. Yang, G. E. Welsch and T. E. Mitchell, "Analytical electron microscopy investigation of the oxide scale on a yttrium-implanted Ni-20%Cr alloy," Mater. Sci. Eng., 69, (1985) 351-357.

26. C. M. Cotell, J. Electrochem. Soc., 134, (1987) 1871-1872.

27. P. Hou and J. Stringer, "Ion-implantation of reactive elements in improving the adhesion of thermally grown Cr_2O_3 scales," (Paper Presented at Spring Meeting of the Materials Research Society, Reno, Nevada, 1988), 205-212.

28. E. W. A. Young and J. H. W. de Wit, "The use of a ^{18}O tracer and Rutherford backscattering spectrometry to study the oxidation of NiAl," Solid State Ionics, 16, (1985) 39-46.

29. E. W. A. Young, J. P. M. van Vliet and J. H. W. de Wit, "The influence of Y and Yb on the oxidation mechanism of NiAl studied with Rutherford backscattering spectrometry," (Paper Presented at 9th International Congress on Metallic Corrosion, Toronto (Canada), 1984).

30. R. A. Collins, S. Muhl and G. Dearnaley, "The effect of rare earth impurities in the oxidation of Cr," J. Phys. F.:Met. Phys., 9, (1980) 1245-1259.

31. E. D. Hondros, "Residuals and Properties," Phil. Trans. R. Soc. Lond., A295, (1980) 9-23.

32. P. Nanni, C. T. H. Stoddart and E. D. Hondros, "Grain boundary segregation and sintering in alumina," Mater. Chem., 1, (1976) 297-320.

33. W. E. King, J. Park, J. L. Routbort and K. C. Goretta, "Effect of Y2O3 Additions on the Plasticity of Sintered Cr_2O_3," Oxid. Met., 29, (1988) 217-223.

34. K. Przybylski, A. J. Garratt-Reed and G. J. Yurek, "High spatial resolution AEM observations of yttrium segregation in chromia scales grown on Co-45%Cr," (Paper Presented at 44th Annual Meeting of the Electron Microscopy Society of America, Albuquerque (New Mexico), 1986), 518-519.

35. K. Przybylski and G. J. Yurek, "The influence of implanted yttrium on the microstructures of chromia scales formed on a Co-45 weight percent Cr alloy," J. Electrochem. Soc:Solid-state science and technology, 135, (1988) 517-523.

36. K. Przybylski, A. J. Garratt-Reed and G. J. Yurek, "Grain boundary segregation of yttrium in chromia scales," J. Electrochem. Soc:Solid-state science and technology, 135, (1988) 509-517.

37. C. M. Cotell, K. Przybylski and G. J. Yurek, "Oxidation Behavior of Chromium and a Chromium-Yttrium Binary Alloy," Fundamental Aspects of High Temperature Corrosion-II, ed. D. A. Shores and G. J. Yurek (Pennington, NJ: The Electrochemical Society, 1986), 103-127.

38. K. Przybylski, A. J. Garratt-Reed and G. J. Yurek, "Observation of coherent perovskite particles in growing chromia films," J. Amer. Ceram Soc., 11, (1986) C264-266.

39. R. P. Elliot, Constitution of Binary Alloys, First Supplement (New York: McGraw-Hill, 1965), 366-367.

40. W. E. King, N. L. Peterson and J. F. Reddy, "Study of the "reactive-element" effect in oxidation of Fe-Cr alloys using transvers section analytical electron microscopy," J. de Physique, C4, (1985) 423-428.

41. S. Matsunaga and T. Homma, "Influence on the oxidation kinetics of metals by control of the structure of oxide scales," Oxid. Met., 10, (1976) 361-376.

42. H. Hindam and D. P. Whittle, "Microstructure, adhesion and growth kinetics of protective scales on metal and alloy," Oxid. Met., 18, (1982) 245-283.

43. K. P. Lillerud and P. Kofstad, "Reoxidation of Chromium with densified Cr_2O_3 scales," Oxid. Met., 17, (1982) 127-139.

44. W. E. King and J. H. Park, "Anion grain boundary diffusion in Cr_2O_3 and Cr_2O_3 doped with Y_2O_3," (Paper Presented at Materials Research Society, Reno, Nevada, 1988).

45. J. H. Park, W. E. King and S. J. Rothman, "Cation grain boundary diffusion in Cr_2O_3 and Cr_2O_3 doped with Y_2O_3," J. Amer. Ceram. Soc., 70, (1987) 880-885.

46. D. Caplan and I. Sproule, "Effect of oxide grain sructure on the high temperature oxidation of Cr," Oxid. Met., 5, (1975) 459-472.

47. W. E. King, K. S. Grabowski and P. M. Baldo, "The effect of Y ion implantation on the oxide growth kinetics in Fe-24Cr," Norman L. Peterson Memorial Symposium - Oxidation of Metals and Associated Mass Transport, ed. M. A. Dayananda, S. J. Rothman and W. E. King (Warrendale, PA: The Metallurgical Society, Inc., 1987).

48. M. J. Grahm, J. I. Eldridge and D. F. Mitchell, "Anion transport in growing Cr_2O_3 and Al_2O_3 scales," submitted to Materials Science Forum, ed. W. E. King (1988).

49. W. C. Hagel, "Anion Diffusion in α-Cr_2O_3," J. Amer. Ceram. Soc., 48, (1965) 70-75.

50. A. Atkinson and R. I. Taylor, "Diffusion of ^{51}Cr Tracer in Cr_2O_3 and Growth of Cr_2O_3 Films," NATO ASI Series B, 129, ed. G. Simkovich and V. S. Stubican (1984), 285-296.

51. D. P. Whittle and J. Stringer, "Improvement in Properties: Additives," Phil. Trans. R. Soc. Lond., A295, (1980) 309-329.